IEEE Access
Multidisciplinary | Rapid Review | Open Access Journal

Received May 16, 2018, accepted June 8, 2018, date of publication June 28, 2018, date of current version August 7, 2018.

Digital Object Identifier 10.1109/ACCESS.2018.2850453

Lyapunov Based Fast Terminal Sliding Mode Q-V Control of Grid Connected Hybrid Solar PV and Wind System

SUBHENDU BIKASH SANTRA[1], (Member, IEEE), KUNDAN KUMAR[1,2], (Member, IEEE), PRAVAT BISWAL[1], (Member, IEEE), AND CHINMOY KUMAR PANIGRAHI[1], (Member, IEEE)

[1]School of Electrical Engineering, KIIT University, Bhubaneswar 751024, India
[2]Laboratory of Electric Systems for Automation and Automotive, Industrial Engineering Department, University of Padova, 35131 Padua, Italy

Corresponding author: Subhendu Bikash Santra (subhendu.santrafel@kiit.ac.in)

ABSTRACT This paper shows the effectiveness of adaptive terminal sliding mode control in grid connected hybrid solar PV and wind system for improvement in error tracking performance under different disturbances. Lead acid battery arrangement is made to support hybrid system. To analyze hybrid system, d-q axis circuit models are independently derived for both PMAC (Permanent Magnet AC) generator and inverter. An adaptive Lyapunov-based rapid terminal sliding mode control is superior over the traditional PI control because of its faster error tracking capability and robustness. Q-V-based inverter control is employed to interface single phase grid and the hybrid system. To substantiate the proposed theory a number of case studies have been conducted like parametric changes of converters, inverter and the changes occurring in the hybrid system. Experimental results of proposed control are obtained from a laboratory prototype of 250 W PMAC and 500W PV hybrid module with 100 ampere-hour battery system. Small-signal stability at different disturbance points are analyzed using dynamic simulations on MATLAB/Simulink.*2014R(b)*. Real time controller is implemented through programming in Lab-VIEW on NI c-RIO 9082.

INDEX TERMS Hybrid System, Lyapunov based fast terminal sliding control, NI c-RIO 9082 (compact reconfigurable input output).

NOMENCLATURE

SOLAR PV

I_d: Diode current in single diode model of PV.
I_{se}: Reverse saturation current.
R_{se}: Lumped Series Resistance.
R_{sh}: Lumped Shunt Resistance.
K: Boltzman Constant.
C_2: Output capacitor to PV panel.

WIND SYSTEM

i_d: Direct axis current.
i_q: Quadrature axis current.
Ψ_f: Magnitude of flux.
ω_r: Mechanical angular speed.
T_e: Electromagnetic torque.
P: Number of Pole.
R_S: Stator resistance.
C_p: Efficiency factor.

BUCK-BOOST CONVERTER

i_L: Inductor current.
V_c: Capacitor Voltage.
L_E: Inductor value.
R_c: Parasitic resistance of capacitor.
R_L: Parasitic resistance of inductor.
V_g: Source voltage to the buck-boost converter.
D: Duty ratio.

1−φ INVERTER AND CONTROL PARAMETER

Z: Load impedance.
r_c: Parasitic resistance of filter capacitor.
r_L: Parasitic resistance of filter inductor.
L: Filter inductor.
α, β : Stationary reference frame parameters.
d-q : direct and quadrature axis parameters.
C_d: Common DC link capacitor.
u_{qn} = Nominal control parameter.

u_{qr} = Robust control parameter.
σ_q = Sliding surface for reactive power.
σ_{dc} = Sliding surface for reactive power.

I. INTRODUCTION

By harnessing energy from unconventional energy radix, prolific unsullied energy which is free of cost can be accorded. However, these unconventional radixes of energy are intermittent in nature owing to the reorienting climatic conditions which disrupts uninterrupted power supply. Genuine power and deduction in storage capacity is allocated by combination of diverse unconventional energy resources which can be a realizable solution to overwhelm imperfections. However, a massive hybrid structure fulfills the load ultimatum, which is needlessly lavish [1]. A miniature hybrid structure is prudential, but it is inadequate to fit to the load ultimatum demand. The ideal gradation of the unconventional energy power entity reckons on the mathematical prototype of system peripherals [2]–[4]. Similarly, with the advancement in manufacture technology of semiconductor, the efficiency of photovoltaic solar (PV) cells have escalated. Cost of PV with higher installed capacity comparatively has fallen. Collating PV systems with the wind systems turbine generators, less conversion efficiency, low power consistency, and exorbitance has discerned drawbacks of the PV system [4]–[7].

This paper abridges mathematical modeling [8], [9] and small signal analysis of PV and wind system [10]–[13]. A singular control technique is essential to control the voltage and frequency as well as extraction of the maximum power [11]. Hybrid structure has complicated restraint structure in part to alliance of two or more divergent power fountains. Control technique of hybrid renewable energy systems to supply power to the outlying autonomous areas has been summarized in this article. A repercussion of aggravation in preserving the stability of grid, power mismatch, power quality, energy management, efficient protection tasks, power control etc. may be resulted due to the tremendous boosting capability of grid tied solar PV and wind generation system [14]. The literature [14]–[16] presents the interpretation of diverse techniques of active and reactive control for the flow of power in the 3 phase grid tied PV system. Voltage source inverter (VSI) is employed for the interfacing of the grid with the solar PV array. Hysteresis band type controllers and proportional integral (PI) controllers are predominant among the controllers. Proportion resonant (PR) controller [24] is implemented in static a-b-c reference framework or PI controller in synchronously moving reference d-q frame. Linear controllers are suitable for less perturbation around stable operating point and can only eliminate steady state error [19], [31]. In [17], anticipative controller based current control strategy is proposed in utilization in synchronously reference frame. Tuning of controllers (PI) are adhered by trial and error method and their attainment declines with change of guiding circumstances. The work reported in [18] focuses on various linear and nonlinear controllers for the control of reactive and active flow of power in the PV inverters evoking d-q current peripherals as changing variables. Thus instead of linearizing the system it is better to investigate non-linear control strategy which aims to derive global asymptotically stable closed loop system. Lyapunov based nonlinear control technique is widely adopted in many literatures [24]–[27]. The major improvement possible in this approach is the correct estimation of region of attraction in stable operating point under sudden disturbances [28]–[32]. Adaptive back stepping approach on lyapunov based control is giving good control for multicellular grid connected single phase inverter [32]. Lyapunov based digital control is adopted for rapid prototyping and online control under dynamic operating condition [26], [27]. Literature [19] renders description on finite time Lyapunov based sliding mode control and the terminal sliding mode control (TSM) control has been delineated in [20]. TSM control handles model uncertainty and yields a chattering free operation as well. The proposed terminal sliding mode controller has high-speed concurrence time anticipated by changing feedback technique and is persevered in charge of error tracking. In this paper after modeling hybrid Solar PV array with modified maximum power point tracking (MPPT) for solar PV, the modeling of VSI is conferred. Control of independent reactive and active power, at inverter side (VSI) with concurrent stabilization of voltage at the dc link and power at point of common coupling (PCC) is acquired by proposed nonlinear control using robust lyapunov based fast terminal sliding mode(LYPSM). It ensures high-speed response and helps in apprehending error to scope the sliding surface in finite time attained through lyapunov's theorem of direct stability. A fast terminal sliding surface (FTSS) has been conceived using virtual state feedback technique to concentrate the apprehended error with it.

This paper is catalogued in seven sections. In section Nomenclature, section-I Introduction, section-II representation of model of PV array and wind system and in section-III small signal stability and control through NI c-RIO 9082 based system is discussed. In section-IV Study of VSI with flexible LYPSM controller is mentioned. Simulation results and diverse test cases including change in short-circuits, solar irradiation, power reference changes, etc. are granted in section-V to focus the admirable performance of the new one. The proposed system is verified in Matlab/Simulink platform. Finally, section-VI concludes the paper.

II. SOLAR AND WIND HYBRID SYSTEM MODELING

Modelling of solar PV and wind system is obvious for dynamic study and stability analysis of hybrid system when connected to grid. Different parts of the dynamic system is modelled separately as explained below and simulated in Matlab/Simulink 2014 (b).

A. PV MODELLING

Single diode model is considered for simplicity in analysis [1], [2]. The photovoltaic solar cells are low-voltage

and high-current generating devices. An equivalent circuit of a single diode solar PV cell in Fig.1 (a) where diode is connected in parallel with a current source with two resistances which are shunt and series resistance. I_{ph} is generated current source and output available current is $I = I_{ph} - I_d - I_{sh}$ where $I_d = I_{se}[\exp(\frac{V+IR_{se}}{nV_t}) - 1]$, $I_{sh} = \frac{V+IR_{se}}{R_{sh}}$. Thus, $I = I_{ph} - I_{se}[\exp(\frac{V+IR_{se}}{nV_t}) - 1] - \frac{V+IR_{se}}{R_{sh}}$ and $V_t = \frac{T_cK}{q}$ where K: Boltzmann constant ($K = 1.38 \times 10^{-23}$J/K). n: diode quality factor R_{se}: lumped series resistance. R_{sh}: lumped shunt resistance. q: charge of the electron ($q = 1.6 \times 10^{-19}$C) I_{sc}: reverse saturation current, Tc: temperature of the operating cell (°C), V: Open circuit PV voltage.

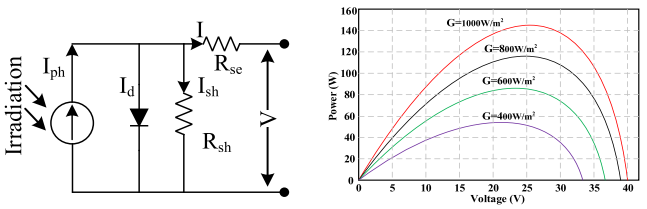

FIGURE 1. (a) Equivalent circuit design of Single diode model of solar cell (b) Power Vs Voltage curve of a solar PV cell.

B. WIND SYSTEM MODELLING

To simplify the response of PMAC it is necessary to transform the equations from the stationary reference frame to d-q axis using Park Transformations. The mathematical model of PMAC can be described in the d-q reference system as follows [2], [3], [13].

$$\left.\begin{aligned} \frac{di_d}{dt} &= \frac{-R_s i_d + L_q P\omega_r i_q + u_d}{L_d} \\ \frac{di_q}{dt} &= \frac{-R_s i_q - L_q P\omega_r i_d - P\psi_f\omega_r + u_q}{L_q} \end{aligned}\right\} \quad (1)$$

$T_e = 1.5P(\psi_j i_q - (L_d - L_q)i_d i_q)$ and $\omega_e = P\omega_r$ where u_d is d-axis voltage, u_q is q-axis voltage, i_d is d-axis current, i_q is q-axis current, R_s is stator resistance, L_d is the d-axis inductance, and L_q is q-axis inductance, ω_r is mechanical angular speed, T_e is electromagnetic torque, ψ_f is magnitude of flux, P is number of pole and J_{eq} is moment of inertia.

The drive transient equation is $\frac{d\omega_r}{dt} = \frac{1}{J_{eq}}(T_e - B\omega_r - T_m)$.

In this paper wind energy system, consists of wind turbine, gear system, rotor, generator, current limiter, rectifier and buck boost converter. It can supply between 10% to 30% of the originalenergy available in the wind. The efficiency factor denoted by C_p can be expressed as:

$C_P = \frac{\text{Power Output by wind terbine}}{\text{Power in the wind}}$ and this can roughly be estimated C_p is 28.8% for simulation purpose [13].

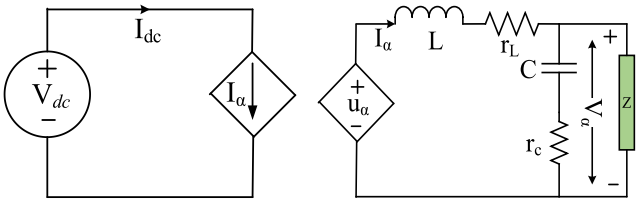

FIGURE 2. Stationary reference frame model of single phase inverter.

C. DC - DC BUCK-BOOST CONVERTER

The state space equations of DC-DC buck boost Converter are given below [6], [7]:

$$\left.\begin{aligned} \frac{d}{dt}\begin{bmatrix} i_L \\ v_C \end{bmatrix} &= \begin{bmatrix} \frac{R_c(1+D) - R_L}{L_E} & \frac{(D-1)}{L_E} \\ \frac{(D-1)}{C} & \frac{(2D-1)}{RC} \end{bmatrix}\begin{bmatrix} i_L \\ v_C \end{bmatrix} + \begin{bmatrix} \frac{D}{L_E} \\ 0 \end{bmatrix} V_g \\ v_o &= -\begin{bmatrix} (1-D)R_c & 1 \end{bmatrix}\begin{bmatrix} \frac{D}{L_E} \\ 0 \end{bmatrix} V_g \end{aligned}\right\} \quad (2)$$

Where I_L is current through inductance L_E, v_C is capacitor voltage, v_o is converter output side voltage, D is duty ratio, R is load resistance V_g is input voltage, R_c and R_L is the parasitic resistance of capacitor and inductor respectively.

D. SINGLE PHASE DC - AC INVERTER

State space average model of the single phase inverter in real and imaginary stationary reference frame [8], [26], [27] is given below and circuit model is shown in fig.12.

$$\left.\begin{aligned} \frac{d}{dt}\begin{bmatrix} I_\alpha \\ I_\beta \end{bmatrix} &= \begin{bmatrix} u_\alpha \\ u_\beta \end{bmatrix}\frac{1}{L} - \begin{bmatrix} I_\alpha \\ I_\beta \end{bmatrix}\frac{1}{L}\left(r_L + \frac{Zr_c}{Z+r_c}\right) - \begin{bmatrix} V_\alpha \\ V_\beta \end{bmatrix}\left(\frac{1}{L} - \frac{r_c}{L(Z+r_c)}\right) \\ \frac{d}{dt}\begin{bmatrix} v_{\alpha c} \\ v_{\beta c} \end{bmatrix} &= \begin{bmatrix} I_\alpha \\ I_\beta \end{bmatrix}\frac{Z}{C(Z+r_c)} - \begin{bmatrix} V_\alpha \\ V_\beta \end{bmatrix}\frac{1}{C(Z+r_c)} \end{aligned}\right\} \quad (3)$$

The d-q model of the inverter can be developed by applying transformation matrix to equation (3) and given below.

$$\begin{bmatrix} X_d \\ X_q \end{bmatrix} = T\begin{bmatrix} X_\alpha \\ X_\beta \end{bmatrix} \quad \text{where, } T = \begin{bmatrix} \cos\omega t & \sin\omega t \\ -\sin\omega t & \cos\omega t \end{bmatrix}$$

and finally neglecting r_L and r_c as in practical they have very small value d-q model of single phase inverter is derived from above equation (3)

$$\left.\begin{aligned} \frac{d}{dt}\begin{bmatrix} I_d \\ I_q \end{bmatrix} &= \begin{bmatrix} u_d \\ u_q \end{bmatrix}\frac{1}{L} + \begin{bmatrix} 0 & -\omega \\ \omega & 0 \end{bmatrix}\begin{bmatrix} I_d \\ I_q \end{bmatrix} - \frac{1}{L}\begin{bmatrix} V_d \\ V_q \end{bmatrix} \\ \frac{d}{dt}\begin{bmatrix} v_d \\ v_q \end{bmatrix} &= \begin{bmatrix} I_d \\ I_q \end{bmatrix}\frac{1}{C} + \begin{bmatrix} 0 & -\omega \\ \omega & 0 \end{bmatrix}\begin{bmatrix} V_d \\ V_q \end{bmatrix} - \frac{1}{CZ}\begin{bmatrix} V_d \\ V_q \end{bmatrix} \end{aligned}\right\} \quad (4)$$

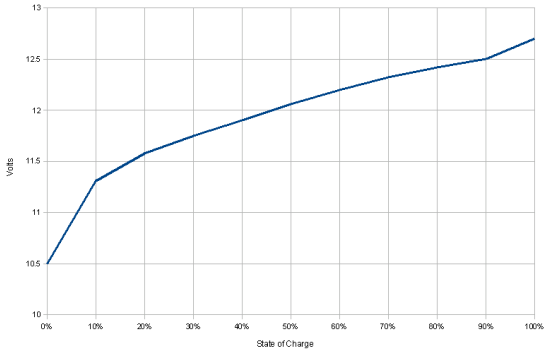

FIGURE 3. State of charge vs terminal voltage.

The dynamic modelling of hybrid system components are required for efficient controller design for both grid integrated mode and standalone mode.

E. SYSTEM ARRANGEMENT

The overall system arrangement is given below in Fig. 4. Wind turbine is connected to gear system which is further coupled with PMAC generator. Output of the wind system is connected to three phase full wave rectifier to convert generated AC voltage to DC voltage. Buck-boost converter is required to regulate output DC voltage from full wave rectifier. PV panel integrated buck boost converter with modified P&O based MPPT controller is adopted to get maximum power. These two sources are then connected to common capacitor C_d. Battery arrangement is required to manage shortage of power from both solar PV and wind system. SOC based control arrangement is made for charging and discharging the battery on availability of power form hybrid system. Solar PV with wind system arrangement is the first stage of hybrid system. Stage 2 is inverter control to feed power to load or grid integration. This scheme is effective in both standalone and grid connected systems. Lyapunov based fast terminal sliding mode control is applied for inverter control for faster response under disturbances. The main objectives of this article are (a) Stabilization of generated hybrid system voltage (b) Effectiveness of proposed fast terminal sliding mode control over classical PI control in grid tied inverter.

III. STABILIZATION OF HYBIID SYSTEM AND CONTROL THROUGH c-RIO

Stabilization of DC link voltage before grid tied inverter is critical in hybrid system. In this work common DC link voltage is considered as 24 volt. By sensing common DC link voltage buck-boost converter is controlled. Tight voltage regulation is adopted to prevent circulating current between two different sources. Here modified P&O based fast acting digital MPPT algorithm is implemented on buck-boost converter connected to the output of PV panel. State of charge based supervisory control helps to select different operating modes in hybrid system. These modes are (a) Normal hybrid mode (b) Semi-hybrid system (c) Battery mode and discussed in Table-1.

TABLE 1. Mode of operation of hybrid system.

Normal hybrid mode	Semi-hybrid mode	Battery mode
When there is no shortage of power available from sources then battery is in charging condition (Fig.11) and capacitor C_d is delivering power to load. $P_{wind}+P_{PV}=P_{charging}+P_L$, where P_{wind} is wind power, P_{pv} is PV panel power, $P_{charging}$ is battery charging power and P_L is load demand.	During non-availability of any one power sources isolation of non power generating unit is important to prevent floating state. In this mode battery can be in charging condition or in discharging condition (Fig.11) $P_{wind}/P_{PV}=P_{charging}+P_L$ or $P_{wind}/P_{PV}+P_{discharging}=P_L$	When both sources are unavailable because of environmental condition then battery unit will provide load demand(Fig.11) . Isolation of non-generating sources is done during this operation. $P_{discharging}=P_L$

PV output voltage and current signal is connected to the analog module channel i.e NI 9225 & NI9227 respectively. These modules are used for sensing PV voltage and current respectively. The digital data is processed through proposed MPPT technique based on simple perturb and observe (P&O) algorithm as shown in Fig. 8.

During non-availability of any power from any power source corresponding source should be isolated from the hybrid system. A simple technique is used to stabilize DC link voltage based on state of charge (SOC) and power availability of sources.

A. BATTERY MODEL AND CURRENT TRACKING

DC link voltage before inverter is important since it is primary source of power which is delivered to load or to grid. Lyapunov based adaptive terminal sliding mode nonlinear control technique is adopted for active and reactive power flow control discussed in section V taking this DC link voltage as a control variable. Maintaining DC link voltage is done primarily through lead acid battery. When sufficient power is available from both PV and Wind system then battery is in charging mode and if any deficiency is observed that would be maintained by the same battery through discharging mode (Fig. 11). For simplicity CIEMAT based dynamic battery model [33] is adopted in this paper. Series capacitor model is used and the terminal voltage.

For $E_{bat} < \eta\, E_g$ $E_{bat}(t) = \eta\, [E_{cb}(t) + E_{cp}(t)]$ and SOC $= (E_{cb}(t) - 2)/0.16$. Whereas, $E_{bat} > \eta\, E_g$, $E_{bat}(t) = \eta\, [E_{cb}(t) + R(t) i_{bat}(t)]$, SOC $= 1$ and, $E_{cb}(t) = 2.16$ V.

$$R(t) = \frac{1}{C_{10}}\left(\frac{6}{1+i_{bat}^{0.6}((t))} + \frac{0.48}{(1-\frac{(E_{cb}(t)-2)}{1.6})^{1.2}}\right)$$
$$C_b(t) = \frac{1.67 C_{10}}{1+0.67\left(\frac{i_{bat}((t))}{I_{10}}\right)^{0.9}} \frac{1}{0.16\eta}, \quad (5)$$

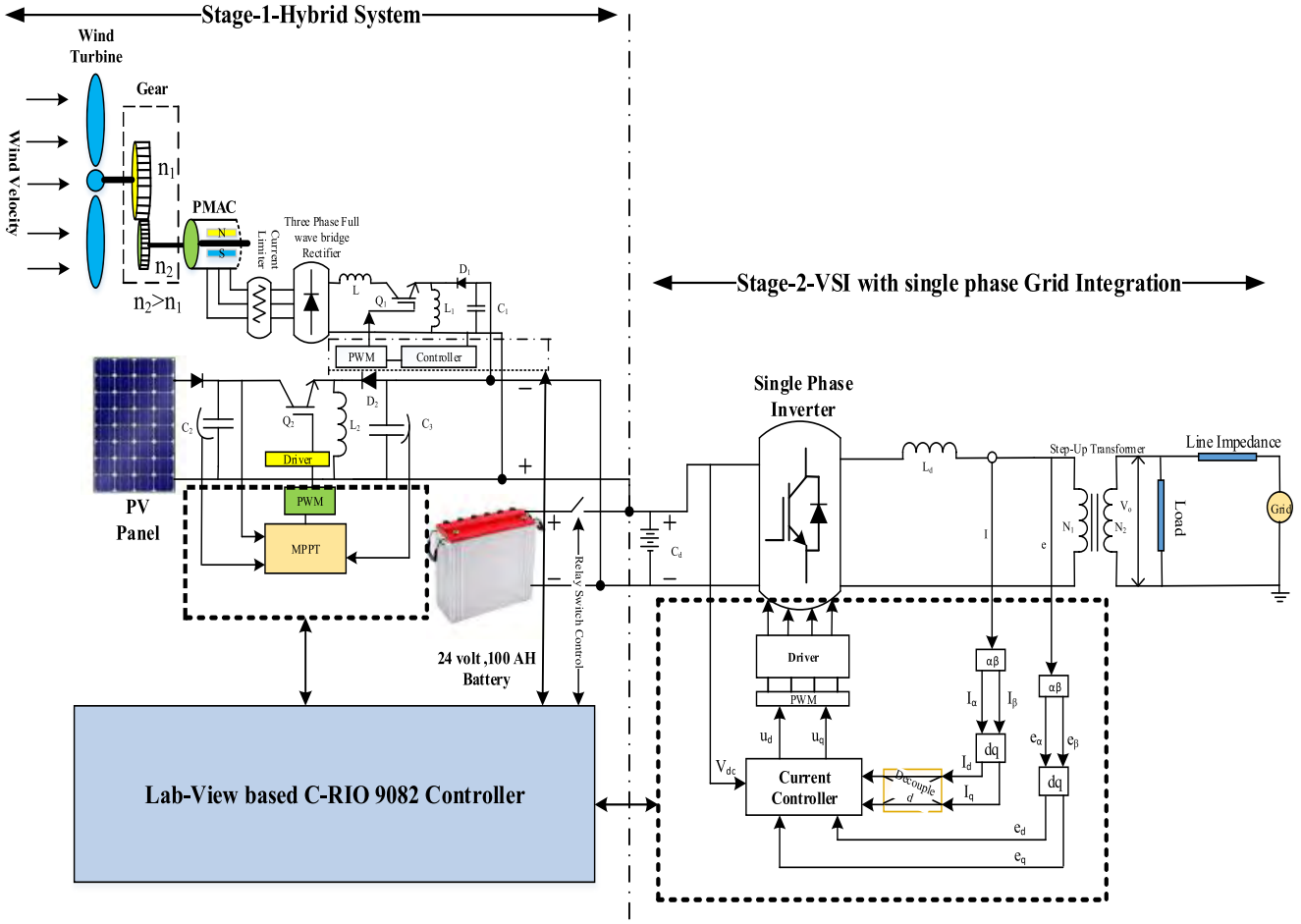

FIGURE 4. Proposed scheme.

And

$$I_{10} = \frac{C_{10}}{10}.$$

$E_{bat}(t)$ = Battery voltage, η = Number of Cells, $i_{bat}(t)$ = Battery. Current (A), E_g = 2.35V E_{cp} = Polarization voltage, E_{cb} = Electromotive force, SOC = Battery State of Charge, R(t) = Internal Resistance. I_{10} = Charge current corresponds to C_{10}. Model parameters are for two lead-acid STECO 3000 batteries. For each battery, the nominal capacity is C_{10} = 100Ah, the nominal voltage is 12V and the number of cells is 6. In the battery pack, the serial/ parallel connection of four batteries is chosen to get a 24V full voltage with two sets in parallel of two batteries in series (see Fig.23 (a)). C_p is chosen as 2000F from model for constant 5amp current.

Battery Current Tracking: The battery current tracking algorithm is shown in Fig. 5. it is designed to determine the current and power references necessary to charge the battery. The estimation of the current and power reference is based on the battery model, which was proposed previously.

- During the battery charging, if the battery current is maintained at a constant high level, the battery voltage increases fast until it reaches gassing voltage (Vg = 2.35V).

During the battery charging, the internal resistor still depends on battery SOC. Its value increases at a high rate when battery SOC is high. In this case, with a constant battery current, the battery losses are more important. Consequently, the battery efficiency is lower.

If the battery is fully discharged and with constant battery current $i_{bmax} = C_{10}/5$, SOC battery can only reach 68%. With constant battery current $i_{bmin} = C_{10}/100$, SOC battery can reach 95% but the charging time becomes longer than before. In order to ensure a high SOC battery, a shorter time charging, an overcharge security and a high efficiency, it is important to reduce battery losses and to keep the battery voltage below the voltage gassing value. This can be achieved through battery current tracking algorithm in Fig.5.

B. MPPT FOR PV SYSTEM

Maximum power point tracking for PV system with simple P&O based technique is reported in many literatures. Higher sampling rate (High resolution ADC) with fast processor can accurately provide duty ratio to the power electronics converter for tracking maximum power from solar PV. But high speed ADC increases cost of the system. Here averaged sampled digital P&O technique is implemented.

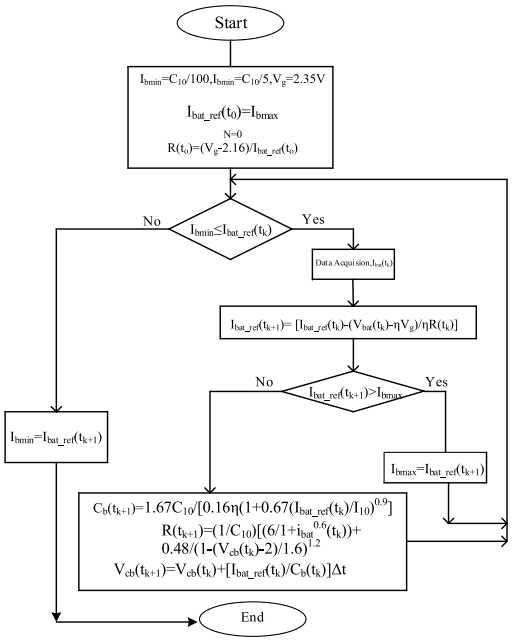

FIGURE 5. Flowchart of battery current tracking algorithm.

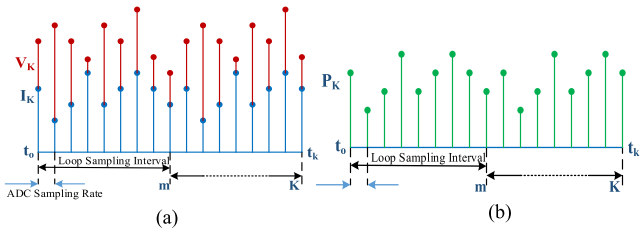

FIGURE 6. Representation of digital data in a pair of sample interval. (b)Representation of power point in the loop sampling interval.

The sampling rate of ADC is higher than sampling rate of digital loop.

Calculation of ΔP requires to have at least two values of power samples.

$$P_{Ka}(avg)|_{\frac{m}{2}} = \frac{P_{K1} + P_{K2} + \ldots P_{m/2}}{m/2}$$

Where, m/2 = (loop sampling per interval)/2, For next samples,

$$P_{Kb}(avg)|_{\frac{m}{2}} = \frac{P_{K1} + P_{K2} + \ldots P_{m/2}}{m/2}$$

The average power in one loop sample interval is

$$P_K(avg)|_m = \frac{P_{Ka}(avg)|_{\frac{m}{2}} + P_{Kb}(avg)|_{\frac{m}{2}}}{2}$$

Similarly, the average value of power in the next loop sampling interval will have the same process followed. Thus the average power in the next consecutive one loop sample interval is $P_K(avg)|_{2m}$.

ΔP is calculated from $P_K(avg)|_{2m} - P_K(avg)|_m$ and checked if $\Delta P > 0$. Then ΔV is calculated. This value of

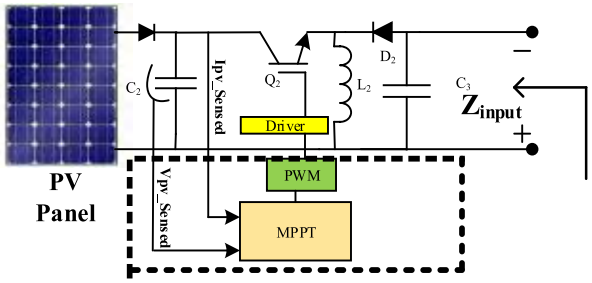

FIGURE 7. MPPT of PV system.

error in voltage is calculated by the same procedure as per the calculation of error in power ΔP.

$$V_{Ka}(avg)|_{\frac{m}{2}} = \frac{V_{K1} + V_{K2} + \ldots V_{m/2}}{m/2}$$

$$V_{Kb}(avg)|_{\frac{m}{2}} = \frac{V_{K1} + V_{K2} + \ldots V_{m/2}}{m/2}$$

$$V_K(avg)|_m = \frac{V_{Ka}(avg)|_{\frac{m}{2}} + V_{Kb}(avg)|_{\frac{m}{2}}}{2}$$

Average voltage in the next consecutive one loop sample interval is $V_K(avg)|_{2m}$.

ΔV is calculated from $V_K(avg)|_{2m} - V_K(avg)|_m$ and checked if $\Delta V < 0$. The error values of both ΔP and ΔV are calculated. The error in Voltage once compared with zero with respect to that the value of duty ratio is calculated i.e Dk as mentioned above flow chart. This digital MPPT ensures faster response and tracks maximum power as shown in Fig.8. These algorithm is implemented in Lab View based programming in NI c-RIO 9082 based system. The capacitor value C2 connected to PV output has a great influence on giving accurate MPPT tracking. If capacitor value is not selected properly then change in voltage due to change in irradiation may not be reflected at output from where voltage sensing is done for MPPT. Here buck-boost converter is connected to PV system. Thus input impedance looking form the load side is required to find out condition for maximum power transfer.

The programmability and online monitoring capability of NI c-RIO 9082 based system makes it suitable for hybrid system monitoring and modelling. The above discussed part ensures the stability of DC link voltage and ensures maximum power is extracted from solar PV system based on dynamic environmental condition on PV panel. Thus hybridization and stabilization is done online through c-RIO based controller which is described in detail in result and discussion section. But it is difficult to integrate this hybrid system to the grid.

Battery Storage is important for hybrid system due to intermittent nature of PV and wind power. Both the renewable sources are incapable of providing constant power over time. Thus battery charging and discharging cycle is required for smooth operation. Total power is sum of wind, PV and storage power. The available power which is fed to the grid is calculated by subtracting source side converter loss from

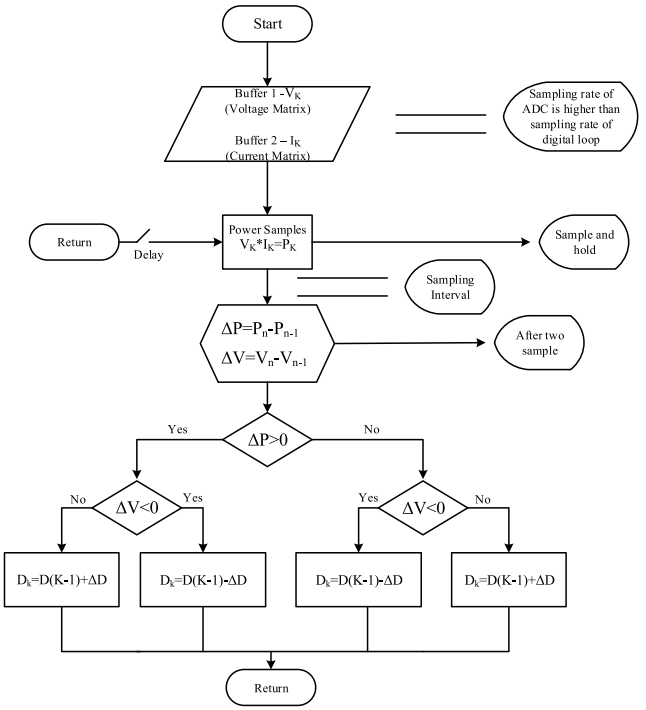

FIGURE 8. Digital P& O algorithm for MPPT.

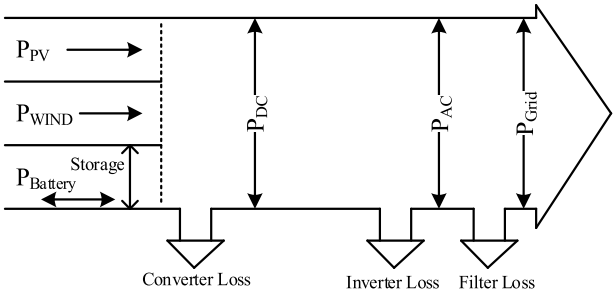

FIGURE 9. Power flow diagram of hybrid system.

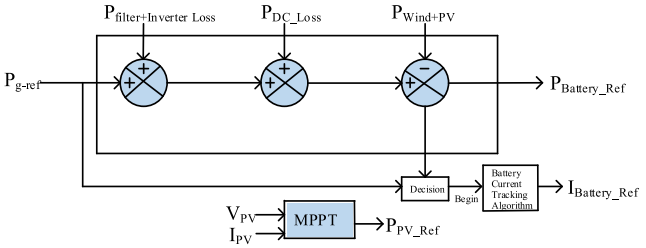

FIGURE 10. Power control diagram of hybrid system.

TABLE 2. System equation.

Power Equation	Control Equation
$P_{PV}=V_{PV}I_{PV}$	$\hat{P}_{PV}=\hat{V}_{PV}\hat{I}_{PV}$ $I_{PV\_ref}=\frac{P_{PV\_ref}}{V_{PV}}$
$P_{Wind}=V_{Buck\_Boost}I_0$	$\hat{P}_{Wind}=\hat{V}_{Buck\_Boost}\hat{I}_0$ $I_{wind\_ref}=\frac{P_{Rectifier\_ref}}{V_{Rectifier}}$
$P_{Battery}=V_{Battery}I_{Battery}$	$P_{Battery\_Ref}=V_{Battery}I_{Battery\_Ref}$
$\left.\begin{aligned}P_g&=V_{sd}i_{sd}+V_{sq}i_{sq}\\Q_g&=V_{sd}i_{sq}-V_{sq}i_{sd}\end{aligned}\right\}$	$i_{sd\_ref}=\frac{P_{g\_ref}\hat{V}_{sd}-Q_{g\_ref}\hat{V}_{sq}}{V_{sd}^2+V_{sq}^2}$ $i_{sq\_ref}=\frac{P_{g\_ref}\hat{V}_{sq}+Q_{g\_ref}\hat{V}_{sd}}{V_{sd}^2+V_{sq}^2}$

the generated power and DC link power is formed. It is responsible for providing power to grid as shown in Fig.9

From the grid power reference power control algorithm is designed as shown in Fig.10. Grid side total power requirement is calculated by taking inverter loss and filter power requirement which are low with grid power reference. This total requirement with DC link power loss gives to DC link power. Battery power reference is calculated after subtracting wind and PV power. Here PV and wind power is not the direct power available from these sources. After subtracting converter loss from direct input power, PV and Wind power is determined. P_{PV_Ref} is determined from MPPT algorithm explained in Fig.8. Battery current tracking algorithm provide I_{bat_ref} to the controller.

Different control variable in input side hybrid system needs to be designed carefully for stabilization as well as proper operation under dynamic condition. Current sensor provides information regarding PV, Wind, and battery power if DC link is maintained constant which is true in steady state. Under dynamic condition error from reference current helps the controller to decide accurate duty ratio of the input side converter to maintain output voltage and power. Control parameter equation of hybrid system is given in table 2 below.

Local Energy flow profile in 24 hours is significant in hybrid system as it provides information regarding charging and discharging requirement of battery. Also it is important to find out PV and Wind power availability over hour since charging of battery is also depend on these power.

The capability of this hybrid system to supply power to grid and to charge lead acid battery depends on the availability of wind and PV power.

Effective management and control of power is possible in three modes as discussed earlier (table-1) (a) Hybrid mode (b) Semi hybrid mode (c) Battery mode. But non-availability of power leads to disconnection from the grid. Fig 11. provides local energy profile of both the sources.

Overall System parameter of hybrid system is given in table 3.

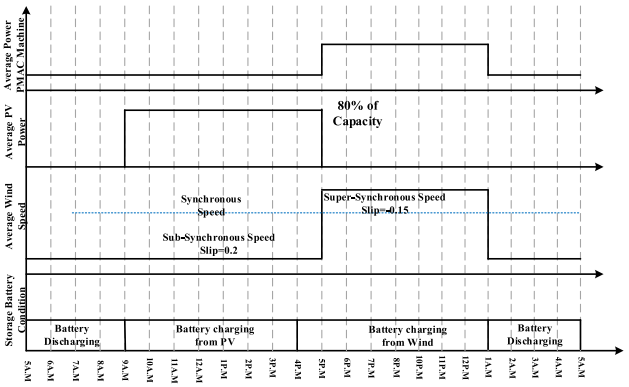

FIGURE 11. Local Energy profile of the proposed wind solar hybrid system.

TABLE 3. Hardware System components.

PMAC System	Storage Battery	Solar PV Module
Type: 3-Phase delta	**Type**: Rechargeable	**Type**:
PM: NdFeB	Pb-Acid.	Polycrystalline.
No of Pole: 4	**Tatal Capacity**:	**Rating**: 500 W
Rated Power: 0.25kW	100Ah	V_{out}/Unit:12V
	$\mathbf{V_{out}}$:12 Volt.	**Output Current**:
		7.5 Amp.
		Operating Temp:
		25℃-35℃

In this paper an adaptive lyapunov based rapid terminal sliding mode control for inverter is adopted for single phase grid integration. The novelty of this method is that it can actually act faster than conventional control available in the literature. In the next section this method is described with suitable control diagram.

IV. LYAPUNOV BASED FAST TERMINAL SLIDING MODE Q-V CONTROL

From the dynamic modelling of inverter explained in section II control technique is designed. PWM modulation is used inverter (VSI) which interface between PV array and grid.The traditional control scheme for active and reactive power flowing from the inverter to the grid is based on the control of the instantaneous direct and quadrature axis components of current. Thus to calculate the active and reactive power flows from the converter a phase frame of reference is used to measure the phase or line voltages and currents. Fig.4 shows schematic diagram of the hybrid system interfaced with load and grid. The interface impedance between PCC and VSI is $R_i + j\omega_e L_i$, where angular frequency. The impedance of line segment between PCC and grid is $R_g + j\omega_e L_g$. Transformed d-q axis current can be written as follows

$$\left.\begin{aligned} pi_{id} &= \frac{-R_i}{L_i} i_{id} + \omega_e i_{iq} + \frac{V_{id} - V_{sd}}{L_i} \\ pi_{iq} &= \frac{-R_i}{L_i} i_{iq} - \omega_e i_{id} + \frac{V_{iq} - V_{sq}}{L_i} \end{aligned}\right\} \quad (6)$$

Where inverter voltage can be written in d-q axis as $V_{id} = \frac{mV_{dc}\cos\delta}{\sqrt{2}}$, and $V_{iq} = \frac{mV_{dc}\sin\delta}{\sqrt{2}}$, where m and δ are the PWM Modulation index and firing angle of Inverter. DC link capacitor voltage dynamics can be written as $\frac{1}{C_d}\frac{dV_{dc}^2}{dt^2} = P_{hybrid} - P_{dc}$, and $P_{dc} = P_t + P_{Loss}$. If inverter loss is neglected for then power from DC source is transferred to inverter bus. Instantaneous active and reactive power is at PCC in d-q reference frame is given as $P_i = V_{sd}i_{sd} + V_{sq}i_{sq}$, $Q_i = V_{sq}i_{id} - V_{sq}i_{iq}$. The instantaneous current in d-q reference frame is expressed as $i_{id} = \frac{P_i V_{sd} + Q_i V_{sq}}{V_s^2}$, $i_{iq} = \frac{P_i V_{sq} - Q_i V_{sd}}{V_s^2}$ and $V_s^2 = V_{sd}^2 + V_{sq}^2$.

For simplified analysis of power flow $V_{sq} = 0$, and $V_{sd} = V_s$ is considered. Thus the active and reactive power flow from the converter becomes $P_i = V_s i_{id}$, and $Q_i = -V_s i_{iq}$ respectively. The dynamics at PCC is written as

$$\left.\begin{aligned} \frac{dP_i}{dt} &= \frac{-R_i}{L_i} P_i - \omega_e Q_i + \frac{1}{L_i}[V_s U_d V_{dc} - V_s^2] \\ \frac{dQ_i}{dt} &= \frac{-R_i}{L_i} Q_i + \omega_e P_i + \frac{1}{L_i}[-V_s U_d V_{dc}] \end{aligned}\right\} \quad (7)$$

Where $U_d = \frac{m\cos\delta}{\sqrt{2}}$, and $U_q = \frac{m\sin\delta}{\sqrt{2}}$.

To avoid some of the problems normally associated with PI controllers, this chapter has explored the use of lyapunov based sliding mode control. Theoretically the robustness of sliding- mode control can ensure accurate tracking performance even in the presence model or parameter uncertainties. However, use of lyapunov direct stability theorem ensures the possibility of adapting the control parameters during a sudden transient change or when the gains appear to be high when the state trajectory approaches the sliding surface. An important requirement of the sliding mode control design is to choose an appropriate sliding surface s(x) for the system state x so that state trajectories will be constrained to lie on it (s(x) 0). However, the discontinuous nature of this control gives rise to chattering phenomenon and thus there is a need to convert the discontinuous control to a continuous one. For designing lyapunov direct stability theorem based controller for the grid connected PV array, the following lemma is followed: For a continuous definite function V(t) to converge to the equilibrium point in finite time the equation given below is satisfied

$$\dot{V}(t) + \beta V(t) + \alpha V^{\gamma}(t) < 0, \quad \forall t > t_0,$$

Hence the time of Convergence is

$$t_{ft} \le t_0 + \frac{1}{\beta(1+\gamma)} \ln \frac{\beta V^{\gamma-1}(t_0) + \alpha}{\alpha}, \quad (8)$$

Where $\alpha > 0$, $\beta > 0$ and $0 < \gamma < 1$

The recommended adaptive FTSM control approach is advantageous correlated to ordinary TSM in terms of driving error remission capability with finite time, fast convergence tract due to altered error trailling and sliding surface model. Tracking errors are considered as follows:

$$e_q = i_{iq} - i_{iq}^*$$

$$e_{dc} = V_{dc} - V_{dc}^*$$

Assuming $\dot{i}^{*}_{iq}$ equals to zero, first derivative of e_q is

$$\dot{e_q} = \dot{i_{iq}}$$

Feedback control law is introduced to implement fast trajectory theory

$$\dot{e_q} = \lambda_q = -\gamma_q \left|e_q\right|^{\lambda 1} \text{sign}\left(e_q\right) \tag{9}$$

Where $\gamma_q > 0$ and $0 < \lambda 1 < 1$ To confirm the stability of feedback control law in Eq.(9)

Lyapunov function $V_q = \frac{1}{2}e_q^2$ is obtained. Stability of Lyapunov function is obtained if

$\dot{V_q} = e_q\dot{e_q} = -\gamma_q \left|e_q\right|^{\lambda_1+1} < 0$ It is to be considered that e_q is not equal to λq, error z_1 is

$$z_1 = \dot{e_q} - \lambda_q = -\frac{R_i}{L_i} i_{iq} - \omega_e i_{id} + \frac{u_q}{L_i} + \gamma_q \left|e_q\right|^{\lambda_1} \text{sign}\left(e_q\right)$$

Control law is expressed as:

$$u_q = u_{qn} + u_{qr}$$

Where u_{qn} = nominal control parameter and u_{qr} robust control parameter

$$u_{qn} = \frac{a_2 i_{iq} - \omega_e i_{id} - \gamma_q \left|e_q\right|^{\lambda_1} \text{sign}\left(e_q\right)}{a_1}$$

Where

$$a_1 = \frac{1}{2\sqrt{2}}\frac{V_{dc}}{L_i} \quad \text{and } a_2 = \frac{R_i}{L_i}$$

Robust control

$$u_{qr} = -k_{qr} z_1 + \int v_q dt,$$

Where

$$v_q = \begin{cases} \rho_{q1}\text{sign}(\sigma_q) + \rho_{q2}\text{sign}(\sigma_q) \\ -\beta_{q1}\lambda_{q1}\left|z_1\right|^{\lambda_{q1}+1}\text{sign}(z_1) \\ -\beta_{q2}\lambda_{q2}\left|z_1\right|^{\lambda_{q2}+1}\text{sign}(z_1);\ z_1 \neq 0 \\ \rho_{q1}\text{sign}(\sigma_q) + \rho_{q2}\text{sign}(\sigma_q);\ z_1 = 0 \end{cases} \tag{10}$$

Where, $\rho_{q1}, \rho_{q2} > 0$; $\beta_{q1}, \beta_{q2} > 0$ and $0 < \gamma_{q1}, \gamma_{q2} < 1$ fast terminal sliding surface is described as

$$\sigma_q = \dot{z_1} + \beta_{q1}\left|z_1\right|^{\lambda_{q1}}\text{sign}(z_1) + \beta_{q2}\left|z_1\right|_{q2}\text{sign}(z_1)$$

Sliding mode control is made adaptive as

$$\beta_{q1} = \rho_{q1}\left|\sigma_q\right|$$
$$\beta_{q2} = \rho_{q2}\left|\sigma_q\right|$$

Similarly derivative of e_{dc} is

$$\dot{e_{dc}} = \dot{V_{dc}}$$

Feedback control law is introduced to implement fast trajectory theory

$$\dot{e_{dc}} = \lambda_{dc} = -\gamma_{dc}\left|e_{dc}\right|^{\lambda_2}\text{sign}\left(e_{dc}\right) \tag{11}$$

Where $\gamma_{dc} > 0$ and $0 < \lambda 2 < 1$

To confirm the stability of feedback control law in Eq. (11)

Lyapunov function $V_{dc} = \frac{1}{2}e_{dc}^2$ is obtained.

Stability of Lyapunov function is obtained if

$$\dot{V_{dc}} = e_{dc}\dot{e_{dc}} = -\gamma_{dc}\left|e_{dc}\right|^{\lambda_2+1} < 0$$

It is to be considered that $\dot{e_q}$ is not equal to λ_{dc}, error z_2 is

$$\begin{aligned} z_2 &= \dot{e_{dc}} - \lambda_{dc} \\ &= \frac{1}{C_{dc}}\left[I_{pv} - \frac{1}{2\sqrt{2}}\left(i_{id}u_d + i_{iq}u_q\right)\right] + \gamma_q\left|e_q\right|^{\lambda_1}\text{sign}\left(e_q\right) \end{aligned}$$

Control law is expressed as:

$$u_d = u_{dn} + u_{dr}$$

Where u_{dn} = nominal control parameter and u_{dr} = robust control parameter

$$u_{dn} = \frac{1}{i_{id}}\left[\frac{1}{a_3}\frac{i_{pv}}{V_{dc}} - i_{iq}u_q + \frac{\gamma_{dc}}{a_3}\left|e_{dc}\right|^{\lambda_2}\text{sign}\left(e_{dc}\right)\right]$$

where,

$$a_3 = \frac{1}{2\sqrt{2}}\frac{1}{C_{dc}}$$

Robust control

$$u_{dr} = -k_{dr}z_2 + \int v_d dt$$

Where

$$v_d = \begin{cases} \rho_{dc1}\text{sign}(\sigma_{dc}) + \rho_{dc2}\text{sign}(\sigma_{dc}) \\ -\beta_{dc1}\lambda_{dc1}\left|z_2\right|^{\lambda_{dc1}+1}\text{sign}(z_2) \\ -\beta_{dc2}\lambda_{dc2}\left|z_2\right|^{\lambda_{dc2}+1}\text{sign}(z_2);\ z_2 \neq 0 \\ \rho_{dc1}\text{sign}(\sigma_{dc}) + \rho_{dc2}\text{sign}(\sigma_{dc});\ z_2 = 0 \end{cases} \tag{12}$$

where, $\rho_{dc1}, \rho_{dc2} > 0$; $\beta_{dc1}, \beta_{dc2} > 0$ and $0 < \gamma_{dc1}, \gamma_{dc2} < 1$ fast terminal sliding surface is described as

$$\sigma_{dc} = \dot{z_2} + \beta_{dc1}\left|z_2\right|^{\lambda_{dc1}}\text{sign}(z_2) + \beta_{dc2}\left|z_2\right|^{\lambda_{dc2}}\text{sign}(z_2)$$

Sliding mode control is made adaptive as

$$\beta_{dc1} = \rho_{dc1}\left|\sigma_{dc}\right|$$
$$\beta_{dc2} = \rho_{dc2}\left|\sigma_{dc}\right|$$

Frequency is obtained from the droop control strategy as

$$f - f_0 = -R_{droop}(P_i - P_{hybrid})$$

where f_o = nominal frequency.

Finally to obtain the control laws for the VSC interface, a positive definite Lyapunov's function is chosen as $V = \frac{1}{2}\sigma_{dc}^2 + \frac{1}{2}\sigma_q^2$. The derivative of V is obtained as follows $\dot{V} = a_1\sigma_{dc} - a_2\sigma_{dc}u_d + a_3\sigma_q - a_4\sigma_q u_q$, hence from lyapunov second law stability of inverter is guaranteed for $\dot{V} < 0$ and to satisfy this condition, the control quantities are to be chosen as

$$\left.\begin{aligned} U_d &= -\frac{a_1 + K_1\sigma_{dc} + K_2\left|\sigma_{dc}\right|^{\lambda}\text{sign}(\sigma_{dc})}{a_2} \\ U_q &= -\frac{a_3 + K_3\sigma_{dc} + K_4\left|\sigma_{dc}\right|^{\lambda}\text{sign}(\sigma_{dc})}{a_4} \end{aligned}\right\} \tag{13}$$

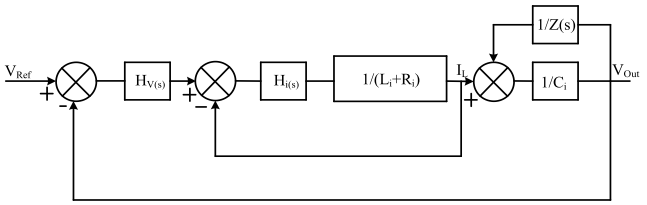

FIGURE 12. Control loop of grid connected inverter.

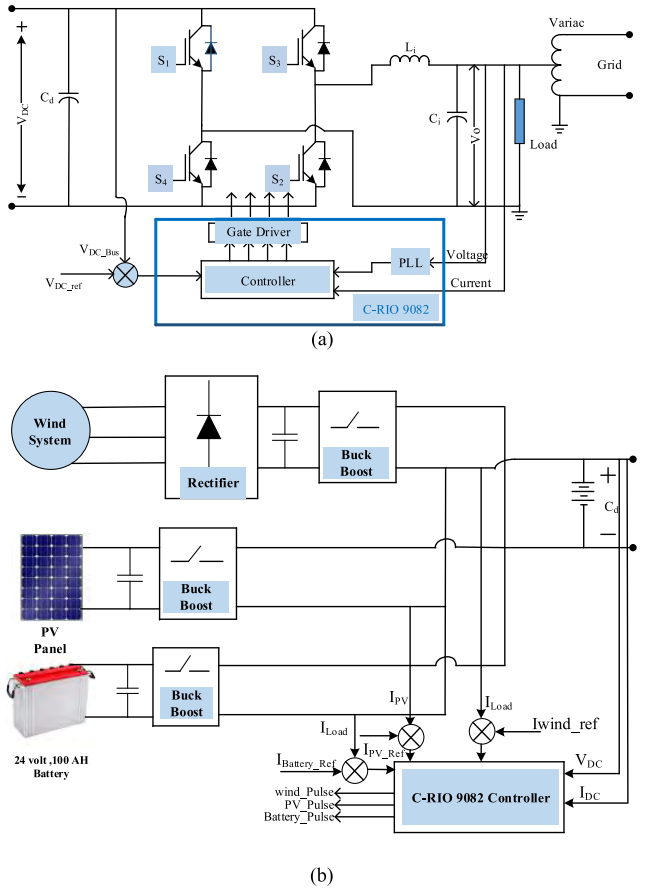

FIGURE 13. Experimental Set-up (a) Inverter side (b) Source side hybrid system.

And

$$\dot{V} = \frac{1}{C_d V_{dc} L_i}(-k_1\sigma_{dc}^2 - k_2\,|\sigma_{dc}|^{\frac{q}{p+1}}\,\mathrm{sign}(\sigma_{dc})) - k_3\sigma_q^2 - k_4\,|\sigma_q|^{\frac{q}{p+1}}\,\mathrm{sign}(\sigma_q)$$

As the lyapunov's function derivative is close to zero, the tracking error will be convergence to the sliding surface, hence a robust controller.

Closed Loop Inverter Control: H(s) represents robust controller. Inner current loop uses filter inductor as a feedback signal. The outer voltage loop utilize the load voltage as a feedback signal.

Droop functions (R_{droop}) are used for grid connection using (P-Q) and (Q-V) slope Here Q-V based robust control is proposed for grid connection. Inverter set has to supply apparent

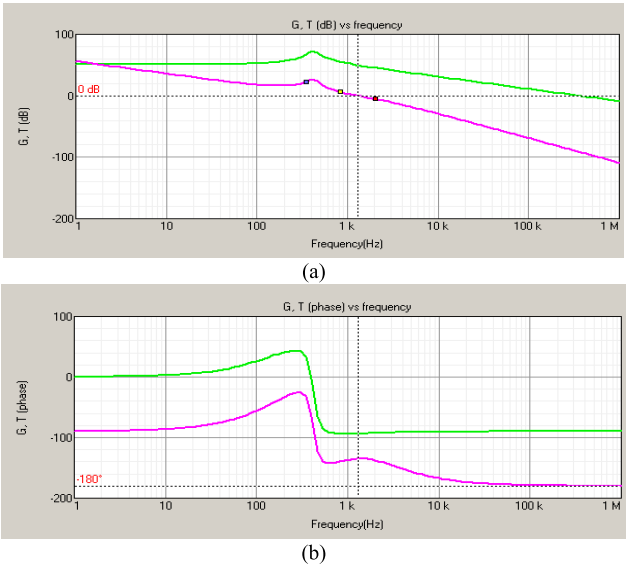

FIGURE 14. Buck Boost Converter (a) Gain plot (b) Phase plot.

TABLE 4. System parameter.

Number of parallel (n_p), series cells, (n_s)	6, 300
Cell's short circuit current, I_{sc}	7.5A
Cell reverse saturation current, I_{rs}	$1.2\text{x}10^{-7}$A
Charge of an electron, q	$1.602\text{x}10^{-19}$C
Boltzmann's constant, k	$1.38\text{x}10^{-23}$J/K
Ideality factor, A	1.92
Cell's reference temperature, θ_{ref}	300^0K
Short circuit current temperature coefficient of cell, K_I	0.0017
Solar Wattage (Table-III)	500W
Wind Wattage (Table-III)	250W
Battery Lead Acid type (Table-III)	24 Volt , 100 Ah

power to grid or to the load. This can be divided into different ways. (a) Inverter exports active power to load and grid, load imports reactive power from grid. (b) Load imports active and reactive power from inverter (c) Inverter provides active and reactive power to both grid and load.

V. RESULT AND DISCUSSION

Overall system is simulated in Matlab/Simulink *2014 R(b)* using mathematical models of the PV array, wind generator, boost converter and the IGBT based VSC converter as shown in Fig.3. Experimental set-up comprises of two sections i.e (a) inverter side (b) source side hybrid system as shown in Fig13. To demonstrate the effectiveness of the proposed lyapunov theory based sliding mode controller in comparison to the

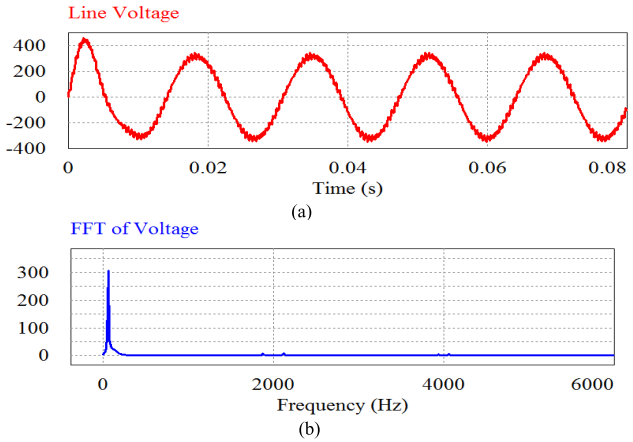

FIGURE 15. (a) Steady state single phase inverter voltage (b) FFT of output voltage.

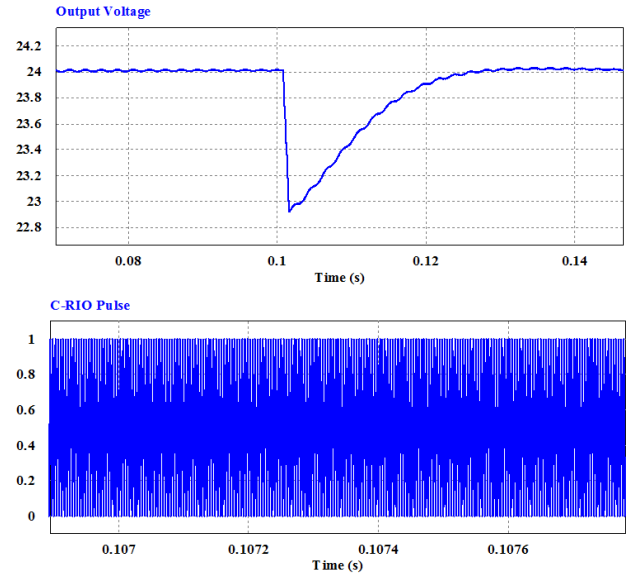

FIGURE 16. Dynamic change of pulse with the change in battery link voltage.

conventional PI controller, different case studies are done as to show that proposed adaptive lyapunov based sliding mode controller is capable to response faster than conventional.

The system data used for simulation study and practical implementation are listed in Table-4. Loop Gain, Phase plot of the compensated buck boost converter is important to find source side system stability when connected to inverter. Figs.14 (a) & (b) the bode and phase plot of the buck boost converter is given. The green line is for stable system after using proper compensator. PLL is used in the control block.

For simulation and hardware realization simple Sine Triangle PWM is used to filter voltage harmonics. In hardware filter circuit is designed as shown in Fig 13-(a). Steady state AC voltage from single phase inverter output for modulation index (M = 0.8) after filter contains less harmonics. Secondary side voltage waveform of transformer is given in Fig. 15(a).

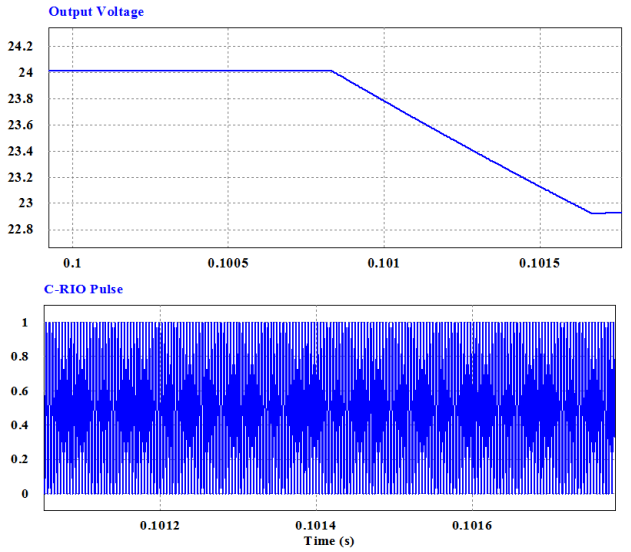

FIGURE 17. Instability of the buck boost converter during energy shortage.

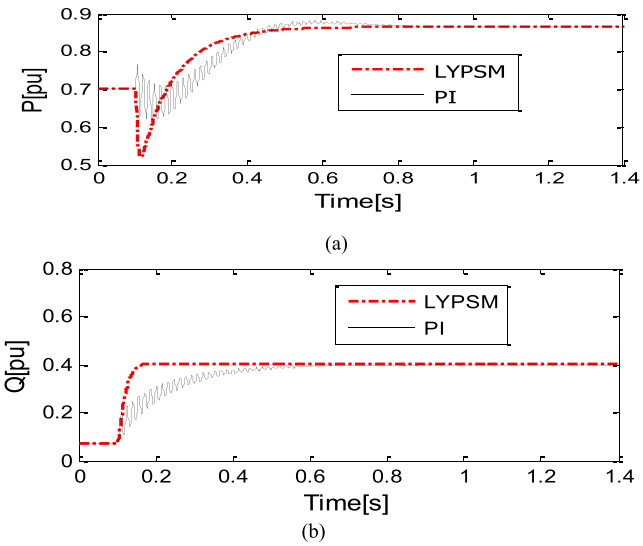

FIGURE 18. Tracking of reference parameters.

There is zero fluctuation in DC link voltage in different modes of hybrid system at steady state. But during changeover from one mode to another fluctuation in DC link voltage is common. Source side converter change duty ratio to maintain DC link voltage. Changes in the DC link voltage due to surplus of energy which is a typical case, pulse width of source side converter changes simultaneously by controller action. Again when step load changes then also DC link voltage changes. Fig. 16 shows the change of PWM pulse on voltage change due to load change. In hardware realization same stabilization of DC link voltage is found as given in Fig. 22 (a) which is close to simulated result.

As discussed in section (III) insufficient energy from solar and wind as well as battery shortage due to environmental condition, source side converter goes to instability.

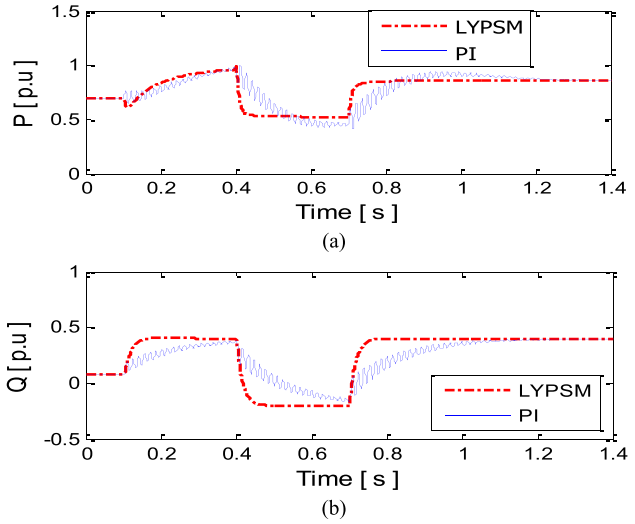

FIGURE 19. Tracking of maximum power for different insolation levels.

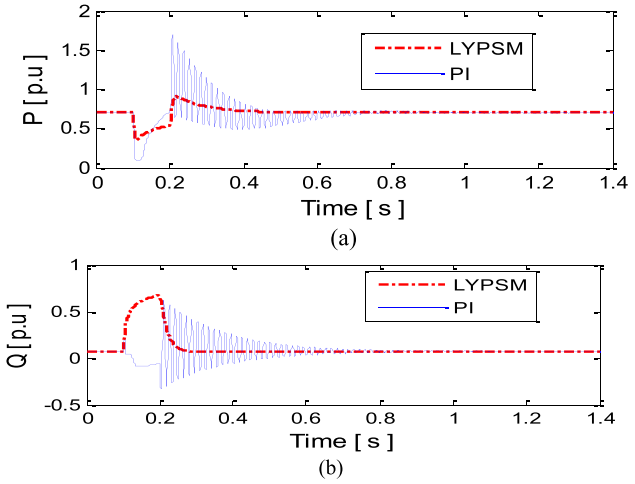

FIGURE 20. Comparision of convergence speed during grid fault.

Fig. 17 shows buck-boost converter operate unstably during this time.

From the simulation and hardware realization it is found that controller is capable of stabilizing the variability in the hybrid system. As discussed in section II only hybrid system stabilization is not important. Inverter (VSI) control for smooth operation while connected to grid is also significant. In this paper lyapunov theory based sliding mode controller is proposed and performs better than conventional PI in different disturbance error tracking point All parameters are taken in p.u. based after inverter for grid integration. Different case studies are considered to show the effectiveness of the proposed control scheme.

Case-1: Tracking capability of both the controllers are examined by applying step commands to P_{iref} from 0.7022 to 0.8658p.u., Q_{iref} from 0.0744 to 0.4p.u. at t = 0.1s respectively as shown in Fig.18. The PI controller gains are

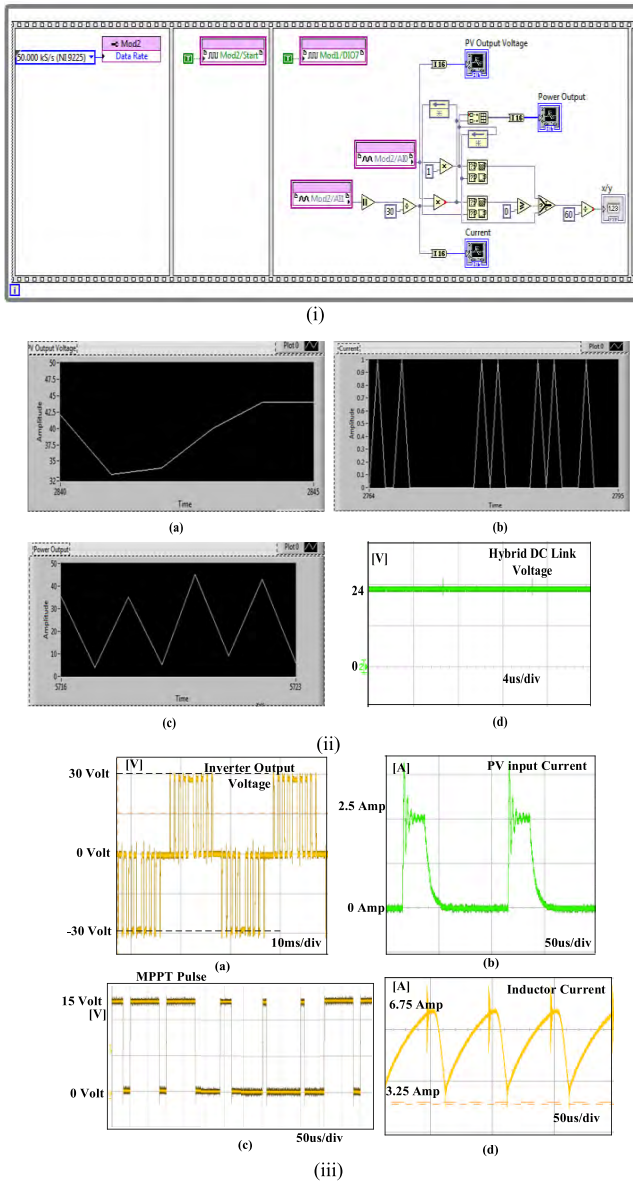

FIGURE 21. (i). Digital Proposed MPPT technique Lab-View Programme, (ii) (a) Online Solar Voltage, (b) Solar Current (c) Solar Power. (iii) Hardware result of the laboratory prototype (a) Inverter Output voltage before filter (b) Solar Current (c) PMMT dynamic pulse (d) Buck-Boost Converter Inductor Current.

obtained using ITAE criterion.

$$\text{PI:}K_p = 75, \quad K_q = -1, \; K_{dc} = -0.73;$$
$$K_{ip} = 3600; \; K_{iq} = -4820$$

The Lyapunov sliding mode controller gains are:

$$\text{LYPSM: } K_p = 150; \quad K_q = 50; \; K_{dc} = -1.0;$$
$$\rho_{dc} = 10.4; \quad \rho_Q = 6.3;$$

For the PI controller the corresponding settling times are 0.8 and 0.7sec respectively. Also it is observed that the PI controller exhibits significant amount of high frequency oscillations before settling to the final value whereas the LYPSM controller settles faster.

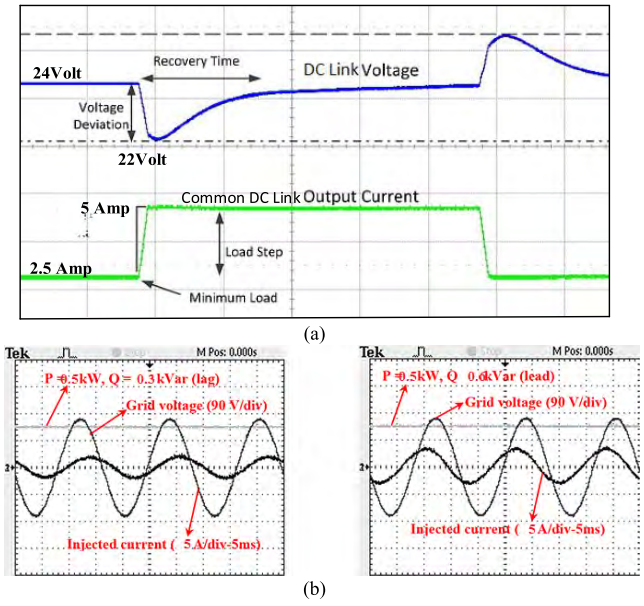

FIGURE 22. (a) Stabilization of DC link voltage with load change. (b)Grid Injected voltage and current.

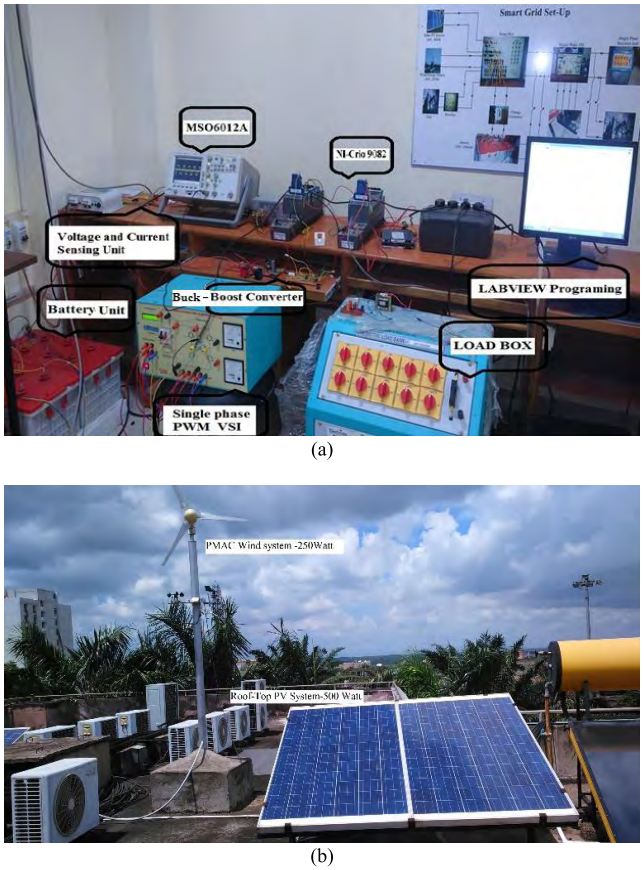

FIGURE 23. (a) Experimental Set Up for hardware realization, (b) Roof-top PV and wind system.

Case-2: At t = 0.1s, there is a step increase in irradiation level from the initial level of 500 W/m^2 (50%) to 900W/m^2 (90%) during a period of 0.1s to 0.4s. From 0.4s to 0.7s the level of insolation is reduced again to 50%. At 0.7s the insolation level is increased to 80% and preserved at that level. Fig.19 shows the transient response of the PV array showing clearly the capability of the LYPSM controller over traditional PI controller.

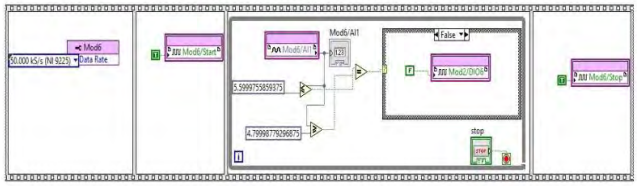

FIGURE 24. Graphical programming for data acquisition.

Case-3: A 3-phase fault is initiated at time t = 0.1sec and cleared at 0.2 sec. Prior to the fault, the values of reference active and reactive powers are: $P_{iref} = 0.7022$ p.u., and$Q_{iref} = 0.0744$ p.u. Fig.20. shows that the controllers are able to come back to the pre-fault after the fault is cleared. As expected the LYPSM controller reduces the oscillations much faster than the corresponding PI controller.

Other system parameters are: $R_i = 15m\Omega$, $L_i = 0.637m\Omega$, $R_g = 10m\Omega$, $L_g = 0.5m\Omega$, $C_{dc} = 0.5$mF. $Q_{base} = 0.3$kVAR, P = 0.5KW, $V_{base} = 230$V, $V_{dc(base)} = 24$V, $R_{droop} = .05$; Based on the simulation result the designed controller is implemented on laboratory based prototype. All the discussion result shows a good match between simulated and hardware findings shown in Fig.21. Sensing circuit for controller design using lab-view (appendix) for the system is presented.

Fig. 23 is the hardware set up, designed for the verification of theoretical findings.

VI. CONCLUSION

This paper a new robust control technique is analyzed and applied to $1-\varphi$grid tied Solar PV and wind hybrid system. Stabilization of hybrid system is done from the information of DC link voltage, current signal from each source side converter with power flow control. MPPT block inside the programme gives maximum power from PV. Total control mechanism is implemented in c-RIO 9082 module. The control approach on sliding mode applying lyapunov's theorem direct stability has been refined in this paper adopting voltage of dc link & reactive power errors. The suggested function of Lyapunov-based nonlinear control is simpler to traditional PI controllers. Furthermore, the spontaneous reactive & active power waveforms are obtained. The simulation results attained from Matlab/Simulink *2014 (b)* based on hybrid Solar PV system model display clearly shows that LYPSM controller yields faster error tracking response in resemblance with PI controller.

APPENDIX

Data Acquisition Programme through Lab-VIEW FPGA interface is given below in Fig 24.

NI-cRIO 9082 Module used for the programming is as follows:
NI 9401: Digital input output module, NI 9225: Analog voltage sensor (300 Volt r.m.s), NI 9227: Analog Current sensor (5 Amp) Inverter MOSFET: IRFZ44N

Buck Boost Converter Inductor: 2 mH for 7.5 Amp maximum current. Switching frequency of buck-boost converter as well as for Inverter is 10 KHz. The control programming of hybrid system is done through Lab-View given below in Fig.25.

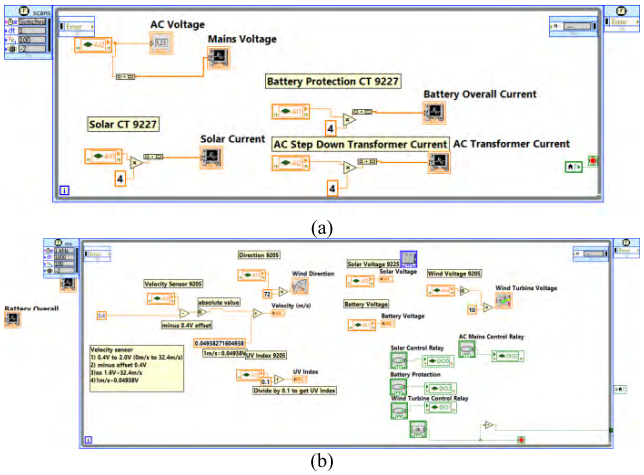

(a)

(b)

FIGURE 25. (a), (b) Control of hybrid system through lab-view.

Discrete Inverter Modelling:

$$\frac{d}{dt}\begin{bmatrix} i_d(t) \\ i_q(t) \end{bmatrix} = A\begin{bmatrix} i_d(t) \\ i_q(t) \end{bmatrix} + B_u\begin{bmatrix} u_d(t) \\ u_q(t) \end{bmatrix} + B_e\begin{bmatrix} e_d(t) \\ e_q(t) \end{bmatrix}$$

Where the matrix definition is given by,

$$A = \begin{pmatrix} -R/L_i & -\omega \\ \omega & -R/L_i \end{pmatrix}, \quad B_u = \begin{pmatrix} 1/L_i & 0 \\ 0 & 1/L_i \end{pmatrix},$$
$$B_e = \begin{pmatrix} -1/L_i & 0 \\ 0 & -1/L_i \end{pmatrix}.$$

The State space discrete model is represented by, $X(K+1) = FX(K) + G_u((K))$ and matrix is represented by $F = (SI - A)^1, G_u = -G_e = \int_0^{T_s} Fd\tau B_u$. Ths the discrete time state equation in grid tied model is represented by,

$$\begin{bmatrix} i_d(k+1) \\ i_q(k+1) \end{bmatrix} = F\begin{bmatrix} i_d((k)) \\ i_q((k)) \end{bmatrix} + G_u\begin{bmatrix} u_d((k)) \\ u_q((k)) \end{bmatrix} + G_e\begin{bmatrix} V_d((k)) \\ V_q((k)) \end{bmatrix}$$

The sampling frequency is selected so that the grid dynamics are significantly below the Nyquist limit associated with the inverter sampling frequency. So, considering vd and vq to be constant during one sample period [27].

$$V_{d,k} \cong V_{d,k-1}, \quad V_{q,k} \cong V_{q,k-1}$$

The above assumption leads to:

$$\left.\begin{aligned} u_{d,k} &= L_i\frac{i_{d,k} - i_{d,k-1}}{T_s} - \omega L_i\left(\frac{i_{d,k} + i_{d,k-1}}{2}\right) \\ &\quad + R\left(\frac{i_{d,k} + i_{d,k-1}}{2}\right) + e_{d,k-1} \\ u_{q,k} &= L_i\frac{i_{q,k} - i_{q,k-1}}{T_s} + \omega L_i\left(\frac{i_{q,k} + i_{q,k-1}}{2}\right) \\ &\quad + R\left(\frac{i_{q,k} + i_{q,k-1}}{2}\right) + e_{q,k-1} \end{aligned}\right\}$$

ACKNOWLEDGEMENT

The authors appreciatively recognize Prof. Debashis Chatterjee of Electrical Engineering dept, Jadavpur University, Kolkata India for his valuable in designing digital control.

REFERENCES

[1] H. Yang, W. Zhou, L. Lu, and Z. Fang,"Optimal sizing method for stand-alone hybrid solar-wind system with LPSP technology by using genetic algorithm," *Sol. Energy*, vol. 82, no. 4, pp. 354–367, Dec. 2008.
[2] C. Wang and M. H. Nehrir, "Power management of a stand-alone wind/photovoltaic/fuel cell energy system," *IEEE Trans. Energy Convers.*, vol. 23, no. 3, pp. 957–967, Sep. 2008.
[3] M. B. Shadmand, M. Mirjafari, and R. S. Balog, "Optimal sizing of photovoltaic-wind hybrid system for community living environment and smart grid interaction," in *Proc. IEEE Energy Convers. Congr. Expo. (ECCE)*, Cincinnati, OH, USA, Oct. 2017, pp. 5545–5552.
[4] L. Xu, X. Ruan, C. Mao, B. Zhang, and Y. Luo, "An improved optimal sizing method for wind-solar-battery hybrid power system," *IEEE Trans. Sustain. Energy*, vol. 4, no. 3, pp. 774–785, Jul. 2013.
[5] S. Sinha and S. S. Chandel, "Review of recent trends in optimization techniques for solar photovoltaic-wind based hybrid energy systems," *Renew. Sustain. Energy Rev.*, vol. 50, pp. 755–769, May 2015.
[6] C. Bhattacharjee and B. K. Roy, "Advanced fuzzy power extraction control of wind energy conversion system for power quality improvement in a grid tied hybrid generation system," *IET Gener., Transmiss. Distrib.*, vol. 10, no. 5, pp. 1179–1189, 2016.
[7] H. M. Al-Masri and M. Ehsani, "Feasibility investigation of a hybrid on-grid wind photovoltaic retrofitting system," *IEEE Trans. Ind. Appl.*, vol. 52, no. 3, pp. 1979–1988, May 2016.
[8] S. Moury, J. Lam, V. Srivastava, and R. Church, "A novel multi-input converter using soft-switched single-switch input modules with integrated power factor correction capability for hybrid renewable energy systems," in *Proc. IEEE Appl. Power Electron. Conf. Expo. (APEC)*, Mar. 2016, pp. 786–793.
[9] B. S. Borowy and Z. M. Salameh, "Methodology for optimally sizing the combination of a battery bank and PV array in a wind/PV hybrid system," *IEEE Trans. Energy Convers.*, vol. 11, no. 2, pp. 367–375, Jun. 1996.
[10] A. C. Luna, N. L. Diaz, M. Graells, J. C. Vasquez, and J. M. Guerrero, "Mixed-integer-linear-programming-based energy management system for hybrid PV-wind-battery microgrids: Modeling, design, and experimental verification," *IEEE Trans. Power Electron.*, vol. 32, no. 4, pp. 2769–2783, Apr. 2017.
[11] M. B. Shadmand and R. S. Balog, "Multi-objective optimization and design of photovoltaic-wind hybrid system for community smart DC microgrid," *IEEE Trans. Smart Grid*, vol. 5, no. 5, pp. 2635–2643, Sep. 2014.
[12] X. Li, D. Hui, and X. Lai, "Battery energy storage station (BESS)-based smoothing control of photovoltaic (PV) and wind power generation fluctuations," *IEEE Trans. Sustain. Energy*, vol. 4, no. 2, pp. 464–473, Apr. 2013.
[13] T. Ma, H. Yang, and L. Lu, "A feasibility study of a stand-alone hybrid solar–wind–battery system for a remote island," *Appl. Energy*, vol. 121, pp. 149–158, May 2014.
[14] R. Logesh, V. Subramaniyaswamy, and R. Logesh, "Resources, configurations, and soft computing techniques for power management and control of PV/wind hybrid system," *Renew. Sustain. Energy Rev.*, vol. 69, pp. 129–143, Mar. 2017.

[15] S. Mane, M. Mejari, F. Kazi, and N. Singh, "Improving lifetime of fuel cell in hybrid energy management system by Lure–Lyapunov based control formulation," *IEEE Trans. Ind. Electron.*, vol. 64, no. 8, pp. 6671–6679, Aug. 2017.

[16] Y. Zhang, K. Tomsovic, S. M. Djouadi, and H. Pulgar-Painemal, "Hybrid controller for wind turbine generators to ensure adequate frequency response in power networks," *IEEE J. Emerg. Sel. Topics Circuits Syst.*, vol. 7, no. 3, pp. 359–370, Sep. 2017.

[17] A. Mohanty, S. Patra, and P. K. Ray, "Robust fuzzy-sliding mode based UPFC controller for transient stability analysis in autonomous wind-diesel-PV hybrid system," *IET Gener., Transmiss. Distribut.*, vol. 10, no. 5, pp. 1248–1257, 2016.

[18] S. B. Santra, S. K. Behera, and C. K. Panigrahi, "Stability analysis and control of hybrid solar and wind system through NI c-RIO," in *Proc. 7th India Int. Conf. Power Electron. (IICPE)*, Patiala, India, 2016, pp. 1–6.

[19] S. Dasgupta, S. K. Sahoo, and S. K. Panda, "A novel current control scheme using Lyapunov function to control the active and reactive power flow in a single phase hybrid PV inverter system connected to the grid," in *Proc. Int. Power Electron. Conf. (ECCE ASIA)*, Sapporo, Japan, 2010, pp. 1701–1708.

[20] C. Meza, D. Biel, D. Jeltsema, and J. M. A. Scherpen, "Lyapunov-based control scheme for single-phase grid-connected PV central inverters," *IEEE Trans. Control Syst. Technol.*, vol. 20, no. 2, pp. 520–529, Mar. 2012.

[21] M. A. Mahmud, H. R. Pota, and M. J. Hossain, "Nonlinear current control scheme for a single-phase grid-connected photovoltaic system," *IEEE Trans. Sustain. Energy*, vol. 5, no. 1, pp. 218–227, Jan. 2014.

[22] H. R. Baghaee, M. Mirsalim, G. B. Gharehpetian, and H. A. Talebi, "Decentralized sliding mode control of WG/PV/FC microgrids under unbalanced and nonlinear load conditions for on- and off-grid modes," *IEEE Syst. J.*, to be published, doi: 10.1109/JSYST.2017.2761792.

[23] J. Liu and A. R. Teel, "Lyapunov-based sufficient conditions for stability of hybrid systems with memory," *IEEE Trans. Autom. Control*, vol. 61, no. 4, pp. 1057–1062, Apr. 2016.

[24] S. Mishra, D. Sharma, Y. Kumar, and D. Pullaguram, "Lyapunov based frequency independent current controller for grid connected single phase PV systems," in *Proc. 7th India Int. Conf. Power Electron. (IICPE)*, Patiala, India, 2016, pp. 1–6.

[25] I. Sefa, S. Ozdemir, H. Komurcugil, and N. Altin, "Comparative study on Lyapunov-function-based control schemes for single-phase grid-connected voltage-source inverter with LCL filter," *IET Renew. Power Gener.*, vol. 11, no. 11, pp. 1473–1482, 2017.

[26] T. Kato, K. Inoue, and M. Ueda, "Lyapunov-based digital control of a grid-connected inverter with an LCL filter," *IEEE J. Emerg. Sel. Topics Power Electron.*, vol. 2, no. 4, pp. 942–948, Dec. 2014.

[27] T. Kato, K. Inoue, and M. Ishida, "Investigation of stabilities of Lyapunov-based digital control for grid-connected inverter," in *Proc. IEEE Energy Convers. Congr. Expo. (ECCE)*, Montreal, QC, USA, Sep. 2015, pp. 2394–2399.

[28] A. Pilloni, A. Pisano, and E. Usai, "Robust finite-time frequency and voltage restoration of inverter-based microgrids via sliding-mode cooperative control," *IEEE Trans. Ind. Electron.*, vol. 65, no. 1, pp. 907–917, Jan. 2018.

[29] H. Yan, X. Zhou, H. Zhang, F. Yang, and Z.-G. Wu, "A novel sliding mode estimation for microgrid control with communication time delays," *IEEE Trans. Smart Grid*, to be published, doi: 10.1109/TSG.2017.2771493.

[30] M. Kabalan, P. Singh, and D. Niebur, "Nonlinear Lyapunov stability analysis of seven models of a DC/AC droop controlled inverter connected to an infinite bus," *IEEE Trans. Smart Grid*, to be published, doi: 10.1109/TSG.2017.2752146.

[31] M. Kabalan, P. Singh, and D. Niebur, "Large signal Lyapunov-based stability studies in microgrids: A review," *IEEE Trans. Smart Grid*, vol. 8, no. 5, pp. 2287–2295, Sep. 2017.

[32] C. Taghzaoui, A. Abouloifa, A. Elallali, A. Hamdoun, Y. Mchaouar, and I. Lachkar, "Adaptive nonlinear control of multicellular single phase inverter," in *Proc. IEEE Int. Conf. Smart Energy Grid Eng. (SEGE)*, Oshawa, ON, Canada, Aug. 2017, pp. 32–37.

[33] J. B. Copetti and F. Chenlo, "A general battery model for PV system simulation," *J. Power Sources*, vol. 47, pp. 109–118, 1994.

SUBHENDU BIKASH SANTRA (M'15) was born in West Midnapur, India, in 1989. He received the M.E. degree in electrical engineering from Jadavpur University, Kolkata, India, in 2012. He was a Research Scholar in power electronics with the Electrical Engineering Department, IIT Kharagpur, from 2013 to 2014. From 2014 to 2015, he was an Electrical Engineer (E&M) with Rail Vikas Nigam Limited (Schedule a PSU under Ministry of Railways, Government of India), where he designed Earth Mat for Elevated Metro Station and Lightning Protection for Station building.

He is currently an Assistant Professor with the School of Electrical Engineering, KIIT University, Bhubaneswar, India. His main research interest is in motor drive, resonant dc–dc converter, and closed loop control in power electronics. He is a member of the Institution of Engineers, India, and a Reviewer of the IEEE TRANSACTIONS ON VEHICULAR TECHNOLOGY and *IET Power Electronics* journals.

KUNDAN KUMAR was born in Godda, India. He received the M. Tech. degree in electrical engineering from the National Institute of Technology Jamshedpur, India, and the Ph.D. degree in electrical engineering from the University of Padova, Italy, in 2010 and 2016, respectively. From 2011 to 2012, he was an Assistant Professor with the Department of Electrical and Electronics Engineering, National Institute of Technology. He was an Associate Professor with the Department of Electrical Engineering, Bengal College of Engineering and Technology, Durgapur, India, from 2016 to 2017. He is currently an Assistant Professor with the School of Electrical Engineering, KIIT University, Bhubaneswar, India. His research interests are power converters, including isolated dc–dc converters, application of wide bandgap semiconductor devices, soft-switching techniques, electric vehicles, and wireless power transfer system. He was a recipient of the Silver Medal for securing first position during his M.Tech. course. He was also a recipient of the Best Presentation Recognition Award at IECON, Japan, in 2015.

PRAVAT BISWAL was born in Bhubaneswar, India. He received the B.Tech. degree in electrical engineering from the C.V. Raman College of Engineering at Bhubaneshwar, Odisha, India, in 2008, and the M.Tech. degree from NIT Warangal specialized in power electronics and drive in 2011.

He is currently a Ph.D. Research Scholar and an Assistant Professor with KIIT University, Odisha.

CHINMOY KUMAR PANIGRAHI was born in Balasore, Orissa, in 1967. He received the B.Tech. and M.Tech. degrees from Sambalpur University, Orissa, in 1990 and 1997, respectively, and the Ph.D. degree from Jadavpur University, Kolkata, in 2007. He has a teaching experience of 20 years of and research experience of five years of his area of interest is power system operation and control, renewable energy systems, and soft computing techniques. Thirteen Ph.D. scholars received the Ph.D. degree under his guidance and four scholars are working at present. He has guided 42 numbers M.Tech. Scholars until now. He has published many papers in referred journals and conferences. He is an active member of different professional societies. He is currently the Professor and the Dean of the School of Electrical Engineering, KIIT University, Bhubaneswar, India.